Millimeter Astronomy

Jeffrey G. Mangum
National Radio Astronomy Observatory
Tucson, AZ

March 15, 2001

To appear in The Encyclopedia of Physical Science and Technology

Abstract

Millimeter astronomy involves the study of astrophysical phenomena through observations at wavelengths from about 0.3 to 4.5 mm (frequencies from about 65 to 900 GHz). Millimeter astronomical investigations are conducted within a wide range of astronomical categories, including planetary astrophysics, studies of the interstellar medium and its inhabitants, and investigations of the properties of external galaxies. Millimeter astronomical observations use the measurements of the emission from dust grains and the spectroscopic signature from interstellar molecules to study the physical, chemical, and dynamical state of the Universe.

Glossary

Correlator: An electronic device which performs the multiplication and averaging of the astronomical signals from a radio telescope. Correlators are used both to process spectral measurements from single antenna telescopes and to process the signals from a collection of electronically-connected telescopes.

Interferometer: A collection of electronically-connected telescopes used to make high spatial resolution astronomical measurements.

Isomerism: The existence of more than one substance having a given molecular composition and mass but differing in structure. For example, HNC is an isomer of HCN.

Jansky: Unit of flux density used in radio astronomy. 1 jansky (Jy) is equal to 10^{-26} W m^{-2} Hz^{-1}.

Contents

Part I
Millimeter Astronomical Observatories

There are two basic types of millimeter astronomical observatory: single antenna facilities and interferometers. Both can be operated either on the surface of the Earth or as space based observatories, although to date only single antenna measurements have been conducted from satellites. Both types of observatory operate in fundamentally the same way, by collecting millimeter wavelength radiation from a celestial object and processing that signal into radiant flux information about the object under study. When a group of two or more single antennas are electronically linked and commanded to observe the same celestial object, the group of antennas has a spatial resolution equivalent to a single antenna with a diameter equal to the separation of the individual elements. This allows millimeter interferometers to make astronomical measurements with very high spatial resolution not easily obtainable with single antenna millimeter telescopes.

Table 1 lists the characteristics of the currently operating millimeter single antenna and interferometer facilities in the world. Note that most of these facilities are located at high altitude sites. This is owing to the fact that millimeter astronomical observations made from the surface of the Earth must contend with the Earth's atmosphere. Many of the molecular constituents of the Earth's atmosphere are very good absorbers of millimeter wavelength emission. Figure 1 shows the millimeter absorption spectrum of the Earth's atmosphere, displayed as signal transmission as a function of frequency. The frequencies in Figure 1 which show low transmission coincide with energy transitions from O_2 and H_2O. The atmospheric scale heights of O_2 and H_2O are approximately 8000 and 2000 m, respectively. Therefore, by locating millimeter astronomical observatories at high altitude sites measurements made with these facilities are less adversely affected by the absorptive properties of the Earth's atmosphere.

Table 1: Millimeter Astronomical Observatories

Name	Location	Latitude (degrees)	Elevation (m)	Telescopes	Diameter (m)	λ (mm)
CSO	Mauna Kea, HI	+19	4000	1	10.4	0.3 – 1.0
IRAM	Pico Veleta, Spain	+37	2920	1	30	0.8 – 3.5
JCMT	Mauna Kea, HI	+19	4000	1	15	0.3 – 0.8
NRAO	Kitt Peak, AZ	+32	1914	1	12	1.0 – 4.5
NRO	Nobeyama, Japan	+36	1350	1	45	1.3 – 15.0
OSO	Onsala, Sweden	+57	24	1	20	3.0, 13.0
SEST	La Silla, Chile	−29	2347	1	15	0.9 – 4.3
SMT	Mt. Graham, AZ	+33	3186	1	10	0.3 – 1.0
UMASS	Amherst, MA	+42	314	1	14	3.0
BIMA	Hat Creek, CA	+41	1043	10	6	1, 3
NMA	Nobeyama, Japan	+36	1350	6	10	1, 2, 3
OVRO	Owens Valey, CA	+37	1216	6	10.4	1, 3
PdBI	Plateau de Bure, France	+45	2560	5	15	1.2 – 3.7
SMA	Mauna Kea, HI	+19	4000	8	6	0.3 – 0.8

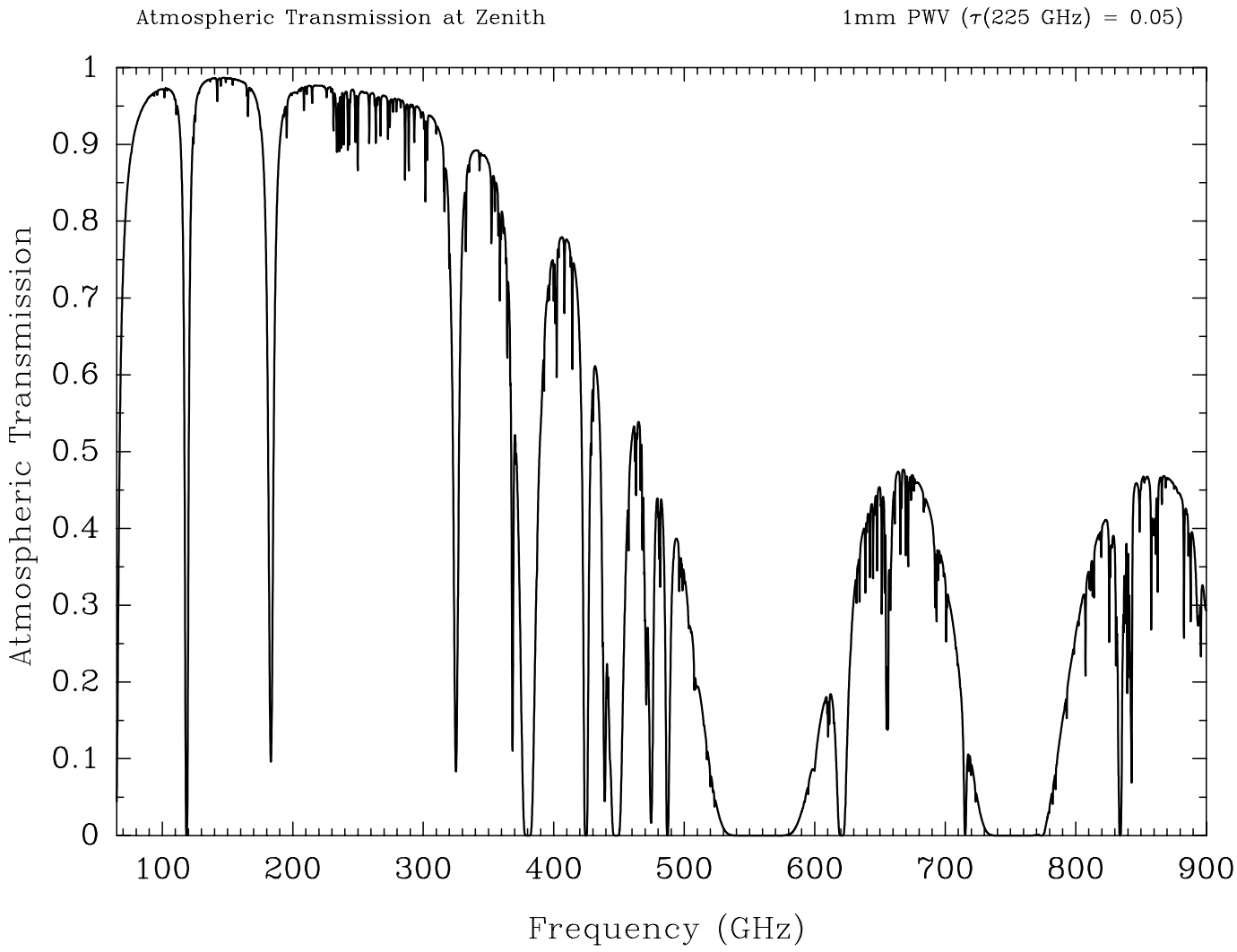

Figure 1: Millimeter emission spectrum from the Earth's atmosphere from an elevation of 4000 meters. The scaling from precipitable water vapor column to atmospheric opacity at a frequency of 225 GHz is shown in the upper right.

Part II
Millimeter Astronomical Observing Techniques

1 Single Antenna Techniques

The basic millimeter single antenna receiving system contains the components shown in Figure 2. Since the astronomical signals which millimeter telescopes are trying to detect are often thousands of times weaker than the atmospheric and instrumental emission which accompanies the astronomical signal, all measurements made with single antennas involve some kind of switching.

1.1 Position Switching

In position switching, the telescope acquires total power measurements at the source position and at a nearby reference position by pointing the telescope and integrating on each position in succession. Since the entire telescope structure must be moved to each position, these measurements are usually made over 30 to 60 second time scales. To produce the final astronomical signal, the individual source and reference measurements are differenced. Figure 3 shows a pictorial representation of a position switched observation. As long as the received signal from the instrumentation or the atmosphere has not changed significantly during the time between a source and its respective reference measurement, position switching will produce reliable astronomical measurements.

1.2 Beam Switching

In beam switching, the telescope acquires total power data at signal and reference positions by repositioning one of the optical components of the telescope system, usually the secondary mirror (see Figure 3). Since the optical components are usually relatively small, they can be switched and positioned accurately at a rapid rate, often several Hz. This allows for rapid switching between source and reference positions, which often allows for bet-

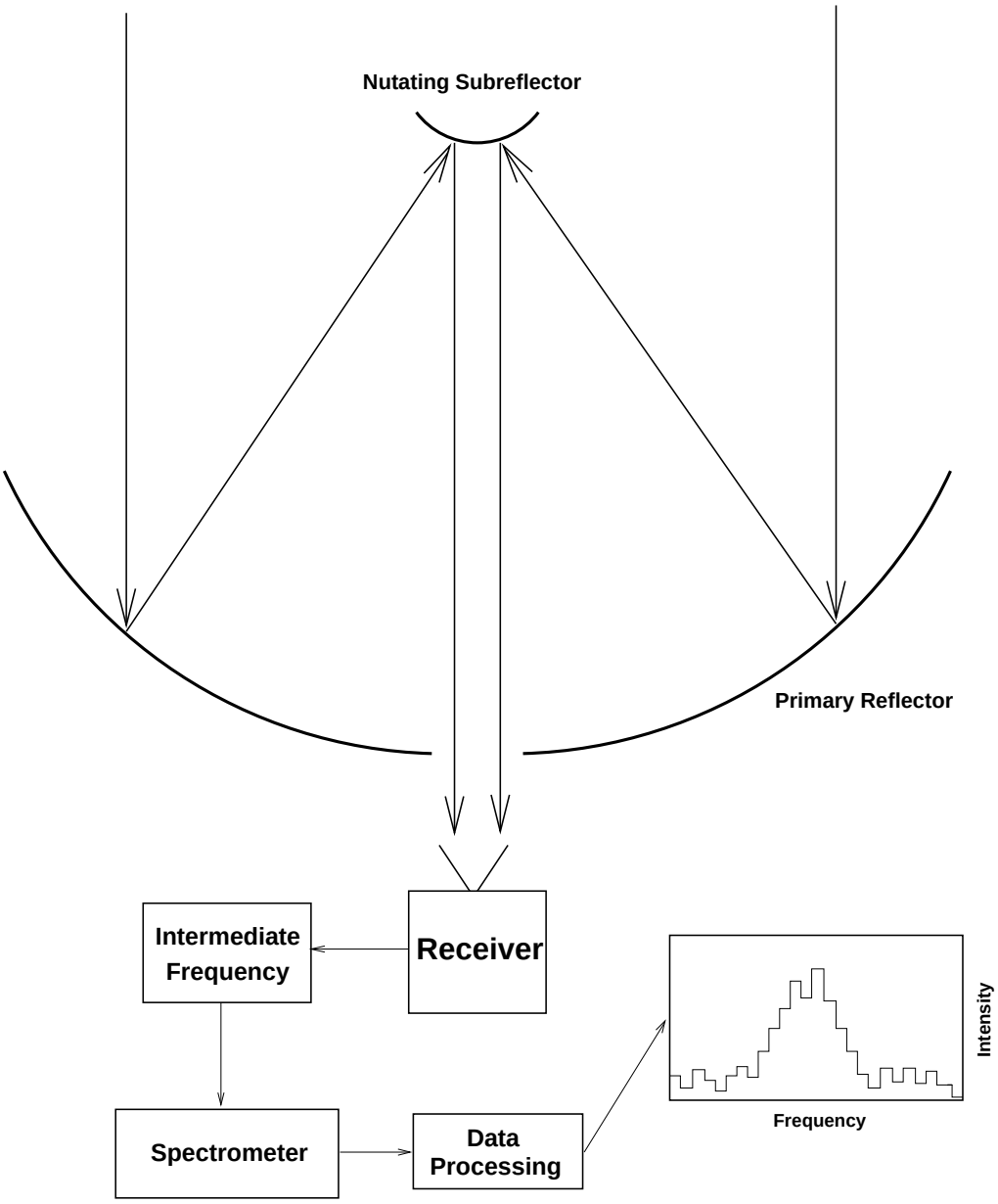

Figure 2: Basic components of the single antenna millimeter observatory. Following signal collection by the primary reflector and nutating subreflector, the receiver amplifies the astronomical signal. The intermediate frequency (IF) then downconverts the received signal to a frequency which can be processed by the spectrometer. The output from the spectrometer, following data processing, is astronomical data.

ter subtraction of the fluctuating emission from the Earth's atmosphere, but is limited by the relatively small reference position offsets attainable with most telescope optics.

1.3 Frequency Switching

In this observing mode, a reference spectrum is obtained by shifting the center frequency of the source spectral measurement. Since it is not necessary to move the telescope or any of the telescope optics, on-source integration time is increased through "in-band" switching. Frequency switching also alleviates the need to find an emission-free reference position when observing in a (spatially) complex emission region. Frequency switching also entails less system overhead than most other observing modes. In principle, frequency switching can be done by switching the frequency of the local oscillator (LO) or an intermediate frequency (IF) oscillator. A pictorial description of frequency switching is shown in Figure 3. If the frequency shift is small enough, usually less than 50 MHz, the spectral line will appear in both the source and reference spectra. When the resultant spectrum is formed, the line will appear twice, once in emission and once in absorption. The spectrum can be "folded" to obtain a $\sqrt{2}$ improvement in signal-to-noise. The primary drawback of frequency switching is that the spectral baselines are generally not as good (flat) as with position or beam switching. This is because the two frequency positions each have their own spectral bandpass shapes which do not cancel in the computation of the final spectrum, thereby leaving a residual standing wave in the overlapped spectrum. A number of techniques, including focus modulation and beam peak scattering, can be used to dampen this residual standing wave.

2 Interferometric Techniques

A basic (two antenna element) interferometer is shown in Figure 4. Measurements with millimeter interferometers are usually done by having all telescopes in the interferometer measure the millimeter signal from an object. The independent but phase coherent signals from each antenna are then multiplied and integrated (together referred to as *correlation*), which results in interference fringes containing the amplitude and phase information of the astronomical signal. As the Earth rotates, the interferometer receives varying

Figure 3: Graphical description of the position, beam, and frequency switching observing techniques.

responses to the structure in the source being measured, and in the process builds up a two (spatial) or three (spatial and spectral) dimensional picture of the astronomical source.

In principle, millimeter wavelength interferometers operate in the same way as centimeter wavelength interferometers, but with the complication that millimeter interferometers are sensitive to atmospheric effects. The varying atmosphere above a millimeter interferometer influences the received signals through absorption and by introducing fluctuations in the received phase of a measurement. Therefore, as with millimeter single antenna observations, it is advantageous to locate millimeter interferometers at high mountain sites. Atmospheric phase fluctuations produce a blurring of the image produced by a millimeter interferometer. Since these atmospheric phase fluctuations seem to depend upon the distance between the antennas, increasing the separation between the antennas in a millimeter interferometer leads to increasingly blurry images for a given level of atmospheric stability.

To correct for the detrimental affects of atmospheric phase fluctuations, a number of correction techniques have been developed. One technique uses a bright point source in the image as a fringe reference point. This technique is often referred to as *self calibration*. Since bright point sources are not always available within a given image, techniques which simultaneously measure the atmospheric emission at wavelengths which provide information regarding the amount of water in the Earth's atmosphere have been developed in recent years. These atmospheric phase correction schemes have proven to be quite successful, allowing for phase corrections which improve the phase noise in a measurement by factors of 2-3. Future improvements in these phase correction systems will likely yield higher levels of improvement to the received astronomical signals.

Figure 4: A basic interferometer. After the signals from an astronomical object are received and amplified by the two antennas, they are combined in a correlator. The correlator multiplies and integrates the two signals, yielding interference fringes which contain the correlated amplitude and phase information from the astronomical source. This information is then processed in a computer to produce an astronomical image.

Part III
Science at Millimeter Wavelengths

3 Star Formation

3.1 Molecular Clouds

As early as the mid-1920's, optical astronomers identified regions in our Galaxy which possessed moderate to high levels of visual extinction. Simple interstellar molecules, such as CH, CH^+, and CN, were discovered in these regions by optical astronomers as early as 1937-41, indicating the presence of an interstellar medium containing regions with densities large enough to support the formation and existence of molecules. The discovery of complex molecules had to await the advent of radio astronomy. In 1968, water (H_2O) and ammonia (NH_3) were discovered toward the regions identified by optical astronomers as having high visual extinction. The existence of these molecules indicated the presence of dense, cool, opaque regions which were eventually recognized as the sites of star formation.

Within the general evolution of spiral galaxies, the star formation process is catalyzed by the continued condensation of gas and dust from the interstellar medium. In this molecular cloud phase, vast regions of the interstellar medium are characterized by high densities, low temperatures, and kinematic motions indicating the existence of infall and outflow. Our Galaxy contains about 10^9 $M_\odot$ of molecular gas. The majority of this gas is located in giant molecular clouds containing approximately 10^{4-6} $M_\odot$ of material. A cloud with support only through kinematic motions of the gas will collapse upon itself if the mass exceeds the Jeans mass,

$$M_J = \left(\frac{\pi k T_K}{\mu m_H G}\right)^{1.5} \rho^{-0.5} \tag{1}$$

while a molecular cloud without pressure support will free-fall collapse on a timescale given by

$$t_{ff} = \left(\frac{3\pi}{32 G \rho} \right)^{0.5} \tag{2}$$

where k is Boltzmann's constant (1.380658×10^{-16} erg K^{-1}), T_K is the kinetic temperature of the gas (K), μ is the mean mass per particle (which is equal to 2.29 in a cloud which is 100% molecular composed of 25% He by mass), m_H is the mass of a hydrogen atom (g), G is the gravitational constant (6.67259×10^{-8} cm^3 g^{-1} s^{-2}), and ρ is the mass density (g cm^{-3}). Since the moderate to high densities and low temperatures found in these giant molecular clouds indicate that most of them should be collapsing, indicating a star formation rate which does not agree with the observed star formation rate, there must be some form of additional support in these regions.

Two mechanisms have been considered as candidates for the additional structural support for molecular clouds; turbulence and magnetic fields. The theoretical and observational investigations into the importance of each of these mechanisms in the physical evolution of molecular clouds currently reach inconclusive results regarding the importance of each.

3.2 Measurements of Physical Conditions

The study of molecular cloud stability and evolution leads naturally to studies of the physical and chemical evolution of the star formation process. Fundamental to this study of the star formation process is the characterization of the physical conditions in the gas and dust comprising these regions. For the gas, volume density n (cm^{-3}), kinetic temperature T_K (K), chemical composition X, turbulent motion Δv (km s^{-1}), and magnetic field strength B (Gauss) are fundamental physical quantities. For the dust, the dust temperature T_d (K), dust volume density n_d (cm^{-3}), and dust opacity κ describe the physical conditions representative of the dust component of a molecular cloud. Note that all of these quantities are dependent upon time and position.

Most of the material in molecular clouds is in the form of H_2, which owing to its lack of a permanent dipole moment has no easily observable rotational transitions. It can be observed through rovibrational and fluorescent transitions, but only within environments which are very specific, such as shocks and regions containing high levels of ultraviolet emission. Therefore, the principal component of molecular clouds is effectively unmeasurable. This

fact forces astronomers to use trace constituents, other molecules and dust, to measure the physical conditions in molecular clouds.

3.2.1 Molecular Emission as a Tracer of Physical Conditions

The primary constituent of molecular clouds, H_2, is also the main collision partner with other molecular inhabitants of these regions. These collisions lead to the excitation of rotational transitions in a variety of molecules, many of which emit at observable millimeter wavelengths. The most abundant molecule after H_2 is carbon monoxide ($^{12}C^{16}O$, usually simply written CO). It was the first molecule discovered at millimeter wavelengths by Wilson, Penzias, and Jefferts in 1970 using the National Radio Astronomy Observatory 36 foot (now 12 meter) millimeter telescope located on Kitt Peak, Arizona. It has been used extensively as a probe of the volume density and kinetic temperature in molecular clouds through measurements of its lowest two rotational transitions at 115.271 and 230.538 GHz. CO has proven to be a very good tracer of the global physical conditions in molecular clouds, but for more compact regions with a larger number of particles along the line of sight (referred to as the column density (N) of a particular molecule), it loses its sensitivity to the bulk of the gas as the opacity in the measured transitions rises. Fortunately, there are other less abundant molecular tracers, including isotopomers (isotopic variants) of CO, such as ^{13}CO, $C^{18}O$, and $^{13}C^{18}O$, which prove to be better probes of these high column density environments.

There are a wide variety of molecules which can be used as tracers of the volume density and kinetic temperature in molecular clouds. The choice of molecular probe depends upon what environment one wishes to study. For example, to measure the physical conditions in the dense cores of molecular clouds, it is best to choose a molecular tracer which is particularly sensitive to the prevalent conditions in this environment. A useful guide used to calculate the sensitivity of a transition to volume density is the *critical density* n_{crit}, which is the volume density required to collisionally excite a transition assuming optically thin conditions

$$\begin{aligned} n_{crit} &= \frac{A_{ij}}{C_{ij}} \\ &= \frac{64\pi^4\nu_{ij}^3}{3hc^3 g_i C_{ij} |\vec{\mu_{ji}}|^2} \end{aligned}$$

$$= \frac{64\pi^4 \nu_{ij}^3}{3hc^3 g_i C_{ij} S \mu^2} \quad (3)$$

where A_{ij} is the spontaneous emission (Einstein A) coefficient for level i, C_{ij} is the collisional deexcitation rate per molecule in level i, g_i is the upper state degeneracy, $|\vec{\mu_{ji}}|$ is the dipole moment matrix element for the transition, S is the line strength for the transition, μ is the dipole moment for the molecule, and the other terms have their usual meanings. Critical densities for common molecules such as CS, HCN, and H_2CO are in the range 10^{4-8} cm^{-3} for a kinetic temperature of 10 K. Therefore, a simple detection of a transition from one of these molecules implies the existence of dense gas. A second consideration is to choose molecules which allow one to derive accurate measures of the volume density and kinetic temperature in a molecular cloud. Since the collisional excitation of molecular transitions is dependent upon the coupled effects of volume density and kinetic temperature, it is often necessary to use molecules which allow one to decouple these effects. The ability to decouple these physical effects depends upon the properties of the molecular structure. There are three basic types of molecules in this regard; linear, symmetric rotor, and asymmetric rotor. Figures 5, 6, and 7 show the energy level structure for these three types of molecules. As can be seen from Figure 5, linear molecules have one ladder of energy levels, the transitions between which are excited by the coupled effects of volume density and kinetic temperature. In general, linear molecules are used to derive the volume density in a molecular cloud by assuming a kinetic temperature or by using a calculation of the kinetic temperature based on measurements of the transitions from another molecule. The energy level structures for the symmetric and asymmetric rotor molecules shown in Figures 6 and 7 indicate a more complex structure. Like linear molecules, the strengths of transitions within a given ladder (designated by the "K" rotational quantum numbers) are dependent upon the coupled effects of volume density and kinetic temperature. A comparison of the strengths of transitions from the same J levels but from different K ladders, though, is dependent only on the kinetic temperature, thus making it possible to derive a decoupled measurement of the kinetic temperature in a molecular cloud. In general, then, symmetric and asymmetric molecules have molecular level properties which, when the appropriate transitions are compared, allow decoupled measurements of the volume density and kinetic temperature in a molecular cloud. Linear molecules do not possess these decoupling properties, thus requiring an independent measurement

of either the volume density or kinetic temperature.

By comparing the measured intensities of a variety of transitions from a given molecule with molecular line intensity predictions from a molecular cloud model, estimates of the volume density and kinetic temperature within a molecular cloud can be made. In general, these estimates reveal that the volume densities in the regions where stars form within molecular clouds exceed 10^4 cm^{-3}, while the kinetic temperatures range from 10 to 300 K. These models also indicate that many molecular cores possess density gradients, suggestive of a structure which could evolve into a collapsing protostar.

3.2.2 Kinematics

The shape of a spectral line is determined by the radial velocity structure along the line of sight through a molecular cloud. The measured widths of spectral lines are generally larger than the thermal width, indicating that the velocity fields within molecular clouds are dominated by Doppler broadening owing to turbulence:

$$\begin{aligned} \Delta v &= v_{therm} + v_{turb} \\ &= 2\sqrt{\frac{2\ln(2)kT_K}{m}} + v_{turb} \end{aligned} \tag{4}$$

where Δv is the full width at half maximum of the spectral line, T_K is the kinetic temperature of the gas, and m is the mass of the particles which make up the molecular cloud (principally molecular hydrogen). Unfortunately, a detailed derivation of the spectral line shape has proven elusive, owing to the effects of kinetic temperature and volume density gradients, spatial structure, and radiative transfer effects within the molecular cloud. Measurements of the line center velocity as a function of position over a molecular cloud do indicate that, in general and on large scales, they are neither collapsing nor rotating. This is not the case on small scales. Evidence for rotation and collapse of molecular cloud cores on 0.1 pc scales have yielded interesting clues to the details of the star formation process. Measurements of cloud core rotation indicate that in magnitude it is only 2% of the gravitational potential energy before collapse, making it relatively unimportant to the overall dynamics of a molecular cloud core.

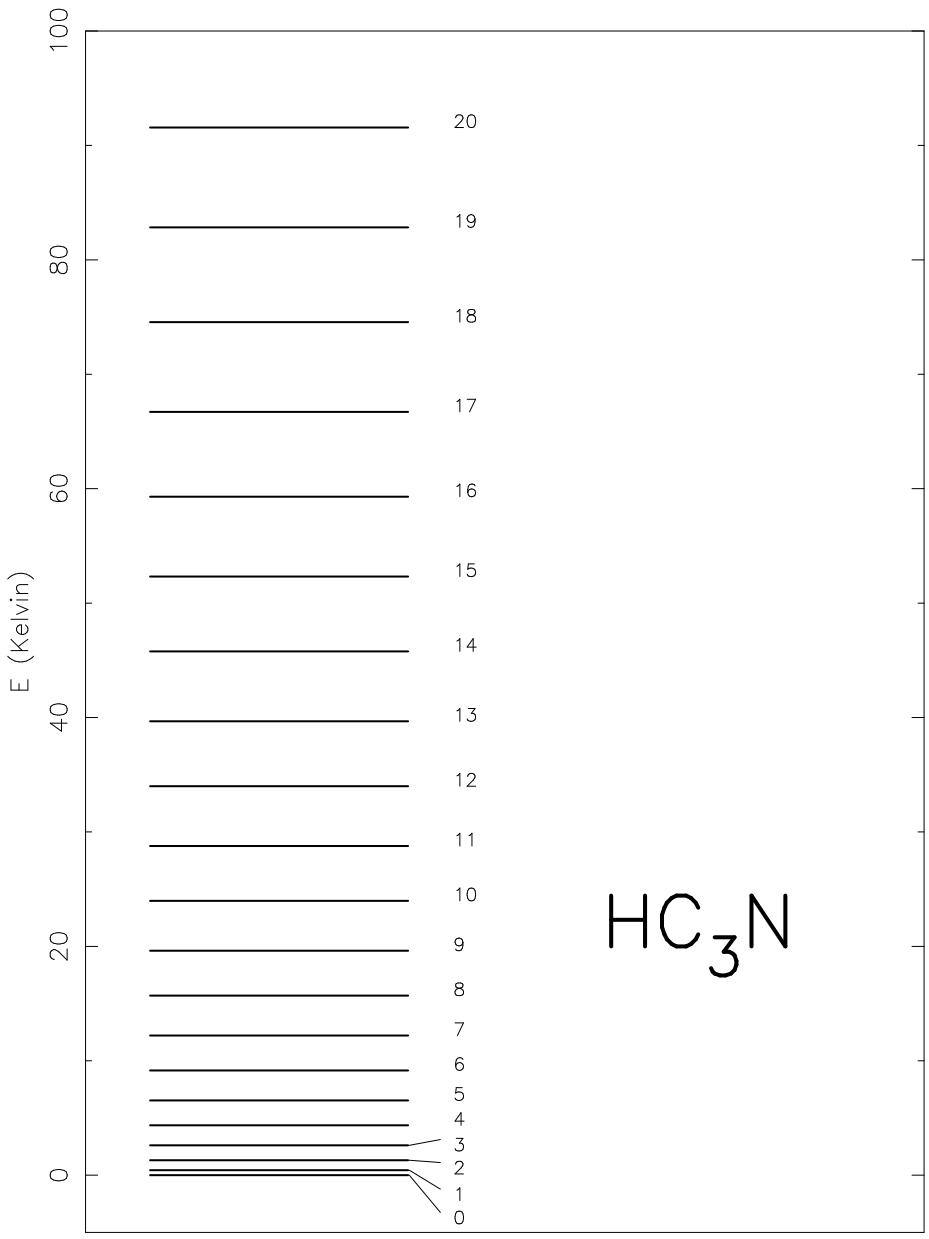

Figure 5: Rotational energy level diagram for HC_3N, a typical linear molecule. The rotational quantum number "J" and associated energy above the ground state are indicated for each level.

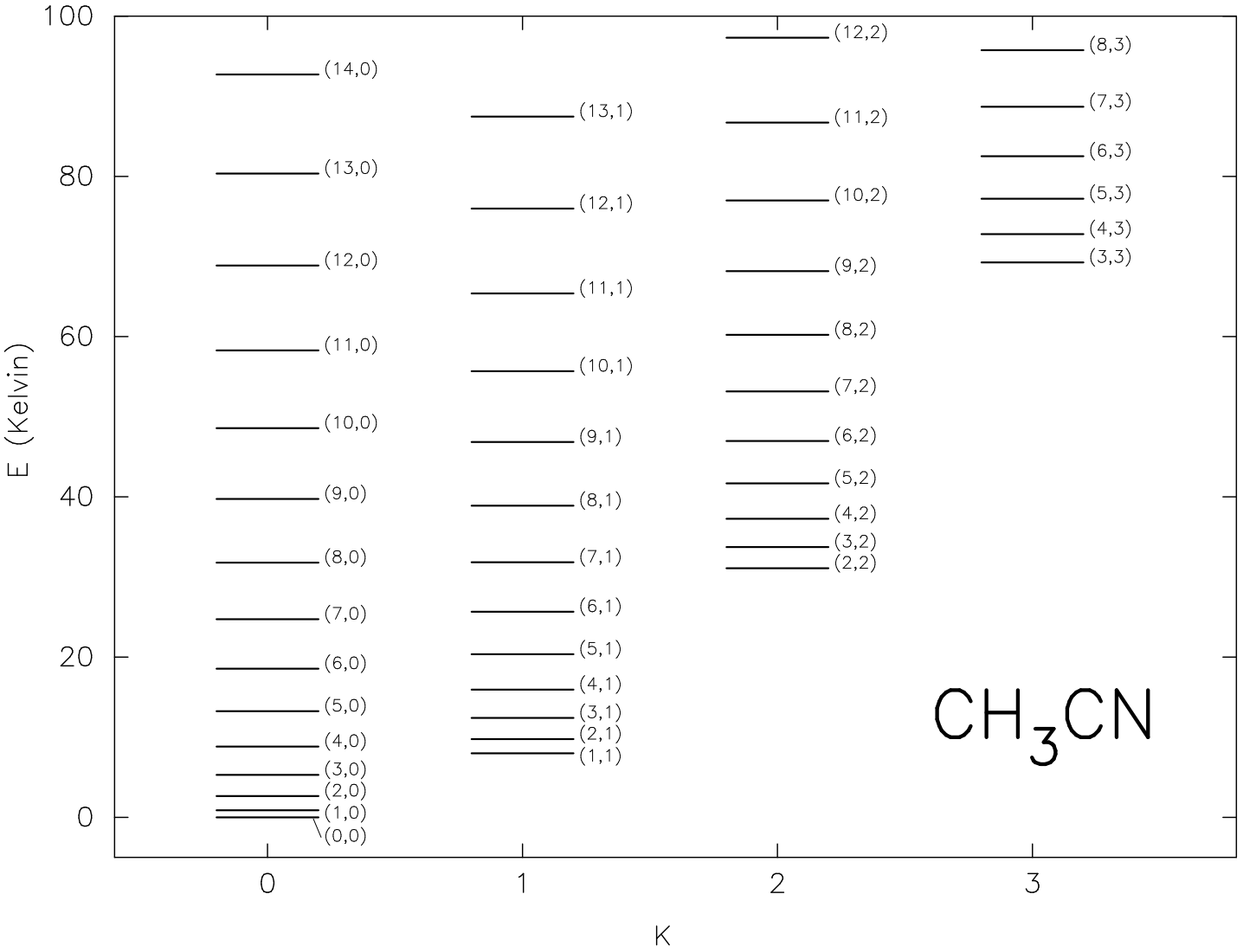

Figure 6: Rotational energy level diagram for CH_3CN, a typical symmetric rotor molecule. The rotational quantum numbers J and K, along with the associated energy above the ground state, are indicated for each level.

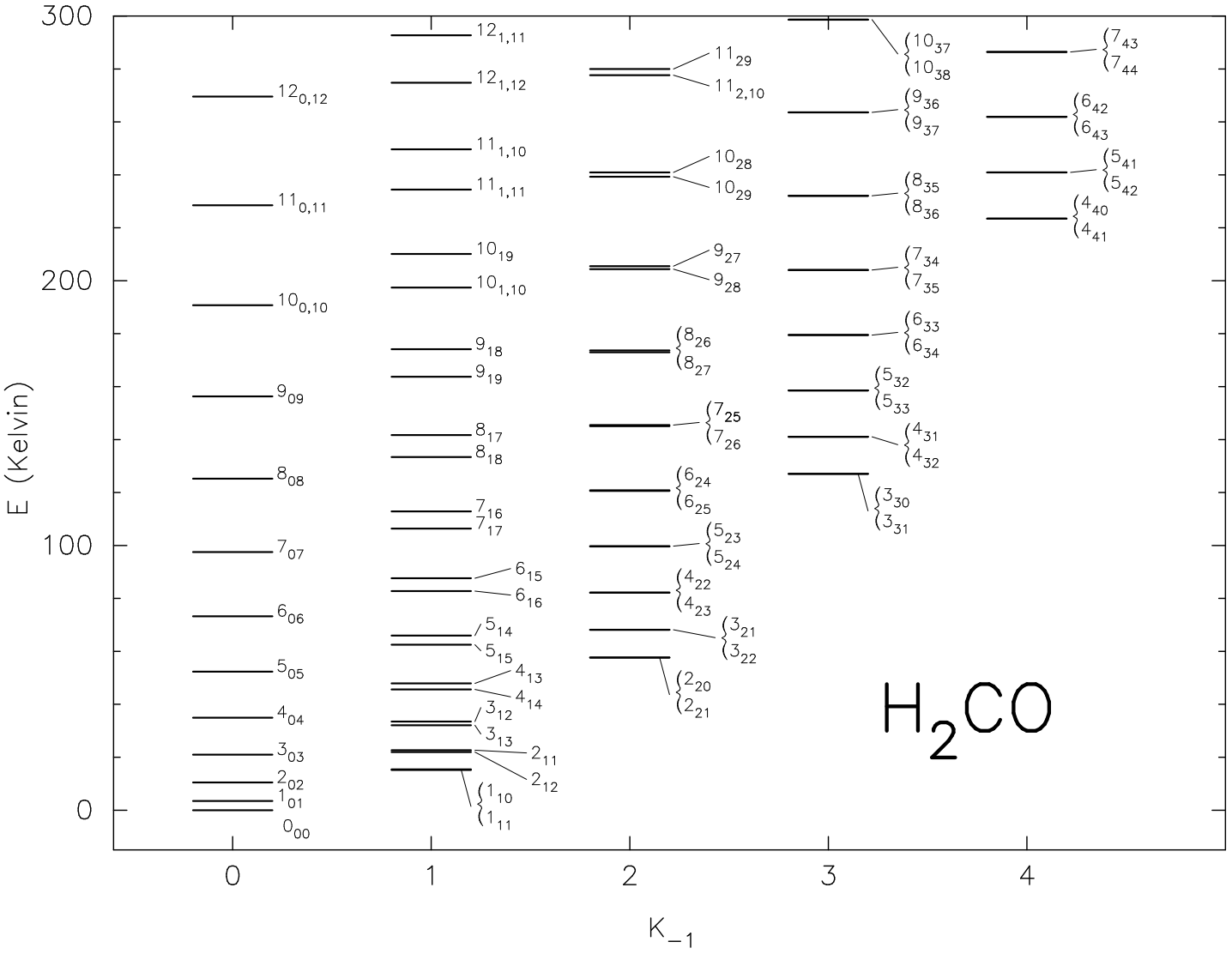

Figure 7: Rotational energy level diagram for H_2CO, a typical asymmetric rotor molecule. The rotational quantum numbers J, K_{-1}, and K_{+1}, along with the associated energy above the ground state, are indicated for each level.

The physical nature of the turbulent component of a spectral line in a molecular cloud is currently a source of considerable debate. Physical processes which have been suggested as sources of the turbulence in molecular clouds are expanding HII regions, supernova remnants, cloud-cloud collisions, galactic differential rotation, and stellar winds. Unfortunately, for all of these processes there are theoretical problems with coupling the energy produced into turbulence.

3.2.3 Magnetic Fields

An understanding of the magnetic field properties of molecular clouds is an important aspect of the overall physical understanding of molecular clouds given their apparent role in providing dynamical support in these environments. There are three methods which have been used to measure the magnetic field strength and direction within molecular clouds: atomic and molecular Zeeman effect splitting, which tell us about the line-of-sight magnetic field component (B_Z); polarization of the emission from dust grains, which gives us information about the component of the magnetic fields perpendicular to the line-of-sight ($B_\perp$); and measurements of spectral line emission polarization, which also tells us about $B_\perp$. Measurements of the Zeeman splitting in atoms and molecules have concentrated on studies of HI, OH, and CN, yielding typical values for B_Z of 10-20 μG within regions with volume densities of approximately 10^3 cm^{-3}. At higher volume densities, magnetic fields as large as 700 μG have been measured. Millimeter dust continuum emission polarization levels of at most a few percent have shown that the magnetic field within the high volume density ($n \geq 10^6$ cm^{-3}) cores of molecular clouds is perpendicular to the major axis of the high density structures (such as disks) and parallel to the outflows associated with these objects. Although the possibility of there being measurable levels of polarization of thermal millimeter spectral line emission has been known for years, it has only recently been detected. The percentage of measured polarized emission is equivalent to that detected through millimeter continuum polarimetry.

Turbulence and magnetic fields cannot simply be applied as independent solutions to the problem of cloud support since turbulence should tangle magnetic fields, thus reducing their effectiveness as a source of support. The theory of magnetohydrodynamic turbulence within molecular clouds has shown that magnetic fields should slow the decay of turbulent motions if these motions are less than the propagation speed along the magnetic field lines,

referred to as the *Alfvén velocity*. However, the stability of magnetic support in the presence of turbulence has been called into question, and the interplay between cloud stability and dynamics drives our understanding of the importance of magnetic fields as a means of molecular cloud support. Future measurements of the magnetic field and direction in molecular clouds should clarify their influence on the overall dynamics and evolution of these regions.

3.3 Dust Emission as a Tracer of Physical Conditions

Dust is also a viable probe of physical conditions in molecular clouds through attenuation measurements at ultraviolet through near-infrared wavelengths and by using measurements of its emission at far-infrared through radio wavelengths. As noted earlier, extinction of background starlight can be used as a probe of the dust column density along the line of sight. Studies of the extinction of optical starlight probe molecular clouds at low extinctions ($A_v \leq 5$), thus giving information about the outer skins of molecular clouds. Recently, surveys of the near-infrared extinction have probed much deeper into molecular clouds, as much as $A_v \sim 30$ magnitudes. These near-infrared surveys have revealed much regarding the inner structure of molecular clouds.

Dust also reveals its presence through emission at millimeter wavelengths. The fact that the opacity of dust continuum emission possesses a power law dependence on wavelength:

$$\kappa_\nu \propto \nu^\beta \tag{5}$$

where $\beta \sim 1 - 2$, allows that dust emission at long wavelengths can trace large column densities in molecular clouds. Millimeter emission from dust can therefore probe larger column densities in molecular clouds, as deeply as $A_v \sim 10^4$ magnitudes. Since the dust emission depends upon the physics of the dust as follows:

$$S_\nu = \frac{2h\nu^3\Omega_s}{c^2}\left\{\frac{1-\exp\left[-\tau_0\left(\frac{\nu}{\nu_0}\right)^\beta\right]}{\exp\left(\frac{h\nu}{kT_D}\right)-1}\right\} \tag{6}$$

where S_ν is the emission flux at frequency ν, Ω_s is the source solid angle, τ_0 is the optical depth at frequency ν_0, β is the dust emissivity power law, and T_D is the dust temperature, an independent estimate of the kinetic temperature within a molecular cloud can be obtained assuming that the gas and dust

are coupled ($T_D \simeq T_K$). The column density and mass of a molecular cloud can also be inferred from dust emission measurements as follows:

$$N = N_\lambda \left(\frac{\lambda}{\lambda_0}\right)^\beta \tau_\lambda \tag{7}$$

$$M = \frac{C_\nu D^2 S_\nu c^2}{2h\nu^3} \left[\exp\left(\frac{h\nu}{kT_D}\right) - 1\right] \tag{8}$$

where C_0 is a coefficient which describes the physical size and millimeter emission properties of the dust grains at frequency ν, D is the distance to the molecular cloud, c is the speed of light, and the other terms have been previously defined. Therefore, measurements of the dust continuum emission from molecular clouds adds complementary physical information to that obtainable through molecular emission measurements.

3.4 Classification of Sources and Evolutionary Scenarios

In order to understand the evolutionary characteristics of the star formation process, it is convenient to have a source classification system. A classification scheme which used the infrared spectral index for $\lambda > 2\mu m$ was developed in the 1980's to characterize infrared sources. This classification scheme contained three categories, Class I, II, and III, which are distinguished by a decreasing amount of emission at longer wavelengths. Once detailed models of the evolution of the star formation process for an isolated low-mass core were developed, these categories became associated with stages in the star formation process. Later, a fourth younger class had to be added to this system, Class 0, when it became apparent that there were a significant number of sources with even larger amounts of emission at longer wavelengths. Figure 8 shows a pictorial description of these classes. Figure 9 shows an integrated CO $2 \rightarrow 1$ emission image from a portion of the Ophiuchus star formation region which contains a rich variety of protostellar and young stellar objects.

3.5 Isolated and Clustered Star Formation Properties

The star formation process is thought to proceed in two different physical environments: isolated regions containing a single, usually lower mass

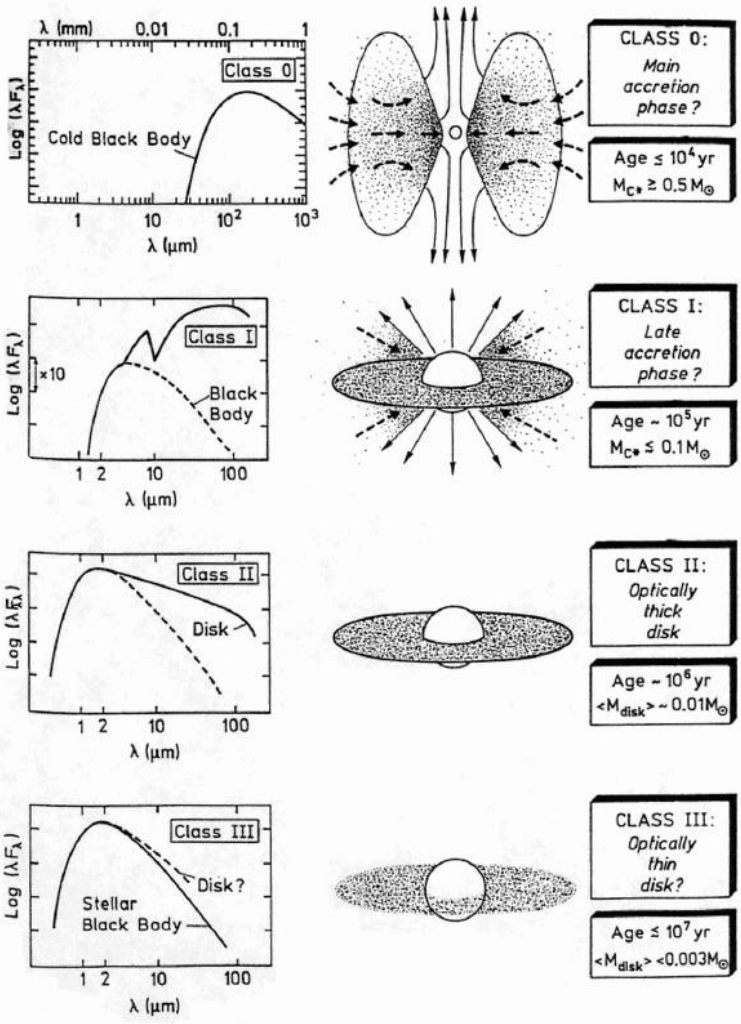

Figure 8: Pictorial description of the star formation evolutionary process. The column on the left of the figure depicts the radiant flux of each Class as a function of frequency. The emission from physically distinct components which compose each Class are indicated. The column in the center of the figure presents a pictorial description of each Class. Arrows indicate mass inflow and outflow. The column on the right of the figure lists the Class name, its primary physical component, its age, and the mass of the central accreting protostar (for Class 0 and I) or the mass of the stellar disk (for Class II and III). From André, P. (1994), *Observations of Protostars and Protostellar Stages*, in Proceedings of the XIIIth Moriond Astrophysics Meeting, The Cold Universe (T. Montmerle, C. J. Lada, I. F. Mirabel, and J. Tran Thanh Van, eds.) Editions Frontiéres, Gif-sur-Yvette, France.

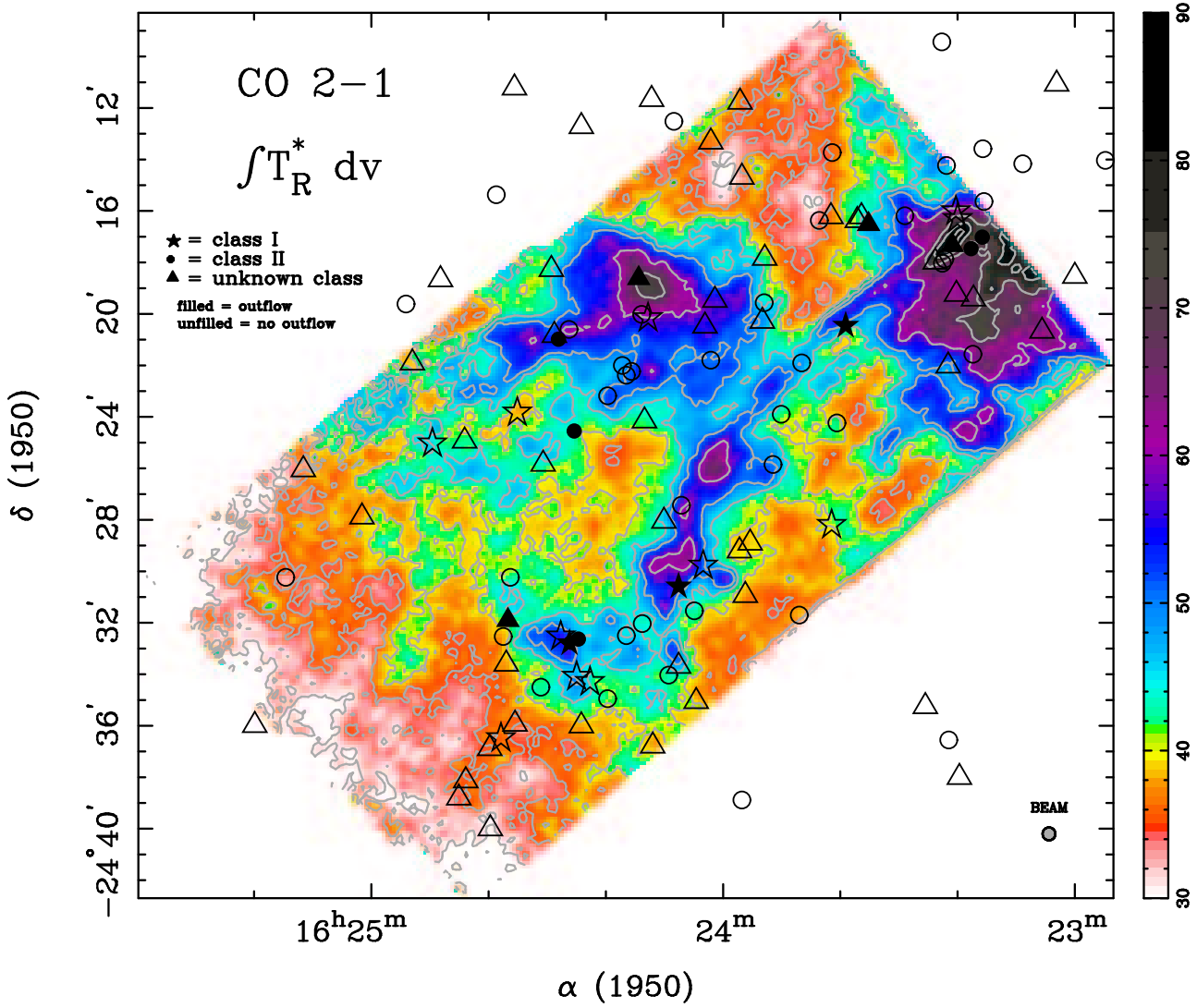

Figure 9: Spectrally integrated CO $2 \rightarrow 1$ emission image of a portion of the Ophiuchus star formation region. The color intensity scale is in K km s^{-1}. Symbols identify the positions of the young stellar objects in the region, some of which possess molecular outflows.

($M < 10M_{\odot}$), object evolving toward the formation of a star, and a group or cluster of dense cores, usually of higher mass ($M \geq 10M_{\odot}$), which appear to be forming stars. The detailed evolutionary sequence described in §3.4 has been developed mainly to explain the isolated star formation process given its simplicity. Observations of the molecular spectral line and continuum emission from these isolated star formation regions are currently being used to test these detailed evolutionary sequences. Specifically, studies of the core collapse signature from spectral line measurements, multi-frequency dust emission measurements of the emission signature from dense cores, and imaging studies of the molecular spectral line and continuum emission from these regions are being used to provide stringent tests of the theories of isolated star formation.

Our understanding of the clustered star formation process is quite a bit different than that for isolated star formation. High mass stars represent a much smaller fraction of the stellar population than low mass stars, so the nearest examples of high mass star formation are far more distant than their low mass cousins. Fortunately, though, stellar luminosity is a strong function of mass, which makes it relatively easy to detect high mass stars at large distances. The quantity of observational information on clustered high mass star formation is equivalent or greater than that from isolated low mass star formation regions. This information is often difficult to interpret, though, owing to the fast evolution of massive stars in a clustered environment, the strong influence that high mass stars exert on their surroundings, and the poor spatial separation of multiple star formation events in these regions afforded by current millimeter astronomical instrumentation. The general picture of low mass protostellar evolution described in §3.4 is likely to be generally valid for high mass star formation in clusters, but the higher densities and more kinematically dynamic environments in which high mass star formation proceeds forces the process to evolve more quickly than in a low mass environment. In general, our overall understanding of clustered star formation is quite a bit more incomplete than it is for isolated star formation, but it is believed that the two evolutionary sequences have many similarities.

4 Evolved Stars

During the evolution of many stars, mass loss during the giant branch phase modifies a star's physical properties. Studies of the stellar envelopes which

result from this mass loss process indicate that evolved stars are a significant contributor of processed material to the interstellar medium. Since this processed material is eventually incorporated into the next generation of stars, an understanding of evolved stars and their mass loss mechanisms is key to understanding the entire star formation process.

Toward the end of their lifetimes, low and intermediate mass stars ($1M_{\odot} \simeq M \simeq 10M_{\odot}$) go through a high mass loss phase. As a result, a circumstellar envelope is formed that can often be detected with spectral line and continuum observations at millimeter wavelengths. These objects include (1) classical Mira and semi-regular variable stars, (2) OH/IR and carbon stars, (3) early spectral type (warm) stars of type B through F, and (4) planetary nebulae (PN). Stellar evolution theory places variables, OH/IR, and carbon stars on the asymptotic giant branch (AGB). These stars lose mass at very high rates of up to 10^{-5} $M_{\odot}$ per year through continuous flows and episodic outbursts. The total galactic rate of mass loss from evolved stars could be as high as 0.35 $M_{\odot}$ per year, making them a significant contributor to the cycle of star formation and the return of processed material to the interstellar medium. The mass loss mechanism in these objects is not well understood, but a prime suspect is radiation pressure on grains which are condensing in the cool extended atmospheres of these objects. Planetary nebulae have evolved beyond the AGB stage, characterized by the ejection and ionization of the star's envelope.

The morphology and extent of circumstellar envelopes is determined by the dynamics of the mass loss process and by the stellar and interstellar radiation field. Since the envelope's density structure is approximately known, the time exposure of the interstellar radiation field can be estimated, and the distribution of molecular photoproducts can be measured. Stellar envelopes represent an unparalleled astrochemistry and radiative transfer laboratory. For this reason, evolved stars have been prime targets for the detection and study of rare molecules in the overall investigation of interstellar chemistry.

5 Chemistry and the Role of Molecules

There are currently 120 known interstellar molecules, 82 of which were discovered at millimeter wavelengths, and the majority of which are organic (see Table 2). Cosmic atomic abundances are generally reflected in the relative abundances of interstellar molecules, with H, C, O, and N being highly im-

portant in molecules. The atomic abundances of S, Si, P, Na, Al, Cl, F, K, and Mg are seen in fewer species, partly owing to reduced abundance and partly owing to inefficient chemistry. Carbon chemistry is the dominant form in the interstellar medium, with long carbon chains playing a dominant role among the organic compounds.

Because of the very low densities and temperatures prevalent in the interstellar medium, molecules cannot be formed by the same processes that produce them on Earth. Astrochemistry appears to be dominated by three chemical reaction regimes: ion-molecule, grain surface, and shock chemistry.

6 Ion-Molecule Chemistry

Gas-phase reactions involving molecular ions are the best understood and are thought to be the most important of the three chemical regimes in the interstellar medium. Ion-molecule chemistry appears to explain fairly well the formation of the simpler interstellar molecules (those containing less than 5 atoms), and recently the formation of a few of the more complex molecules have been explained by ion-molecule reactions.

7 Grain Surface Chemistry

Catalytic reactions on the surfaces of interstellar dust grains, followed by release into the gas phase, can explain the formation of the most abundant molecule, H_2, and appears to be successful at explaining the formation of many of the more complex interstellar molecules. Unfortunately, grain chemistry processes are poorly understood and difficult to simulate. Grain surfaces are also recognized as repositories for many interstellar molecules which may have been produced during a cooler and denser phase of the parent molecular cloud. These grain repositories are thought to be composed of grain surface ices, which when warmed by a nearby star formation event release the stored molecules into the interstellar medium.

8 Shock Chemistry

Strong shocks produced by the expanding ionized envelopes of massive stars and supernova remnants heat and compress the interstellar medium, lead-

Table 2: Known Interstellar Molecules (January 2001) (Courtesy Barry Turner)

Inorganic Molecules (Stable)				
Diatomic		Triatomic	4 Atom	5 Atom
H_2	HCl	H_2O	NH_3	SiH_4
CO	PN	H_2S		
CS	NaCl	SO_2		
NO	AlCl	OCS		
NS	KCl	N_2O		
SiO	AlF			
SiS	HF			

Organic Molecules (Stable)			
Alcohols	Aldehydes and Ketones	Acids	Hydrocarbons
CH_3OH	H_2CO	HCN	C_2H_2
CH_3CH_2OH	CH_3CHO	HCOOH	C_2H_4
	H_2CCO	HNCO	CH_4
	$(CH_3)_2CO$		
	HCCCHO		
	$HOCH_2CHO$		
Amides	Esters and Ethers	Organo-sulfur	
NH_2CHO	CH_3OCHO	H_2CS	
NH_2CN	$(CH_3)_2O$	HNCS	
NH_2CH_3		CH_3SH	
Derivatives			
Paraffin	Acetylene	Other	
CH_3CN	HC_3N	CH_2NH	
CH_3CH_2CN	CH_3C_2H	CH_2CHCN	
		C_6H_6	

Unstable Molecules					
Radicals		Ions	Rings	Carbon Chains	Isomers
CH	C_3H	CH^+	SiC_2	HC_5N	HNC
CN	C_3N	HCO^+	C_3H_2	HC_7N	CH_3NC
OH	C_3O	N_2H^+	C_3H	HC_9N	HCCNC
SO	C_4H	$HOCO^+$	C_2H_4O	$HC_{11}N$	HNCCC
HCO	C_5H	HCS^+	SiC_3	CH_3C_3N	MgNC
C_2	C_6H	H_3O^+		CH_3C_4H	MgCN
C_2H	C_2S	$HCNH^+$		CH_3C_5N	NaCN
C_3	C_3S	H_2D^+		SiC_4	
HNO	CH_2CN	HOC^+		H_2CCC	
CP	SiC	SO^+		H_2CCCC	
SiH_2	CH_2	CO^+		C_7H	
NH_2	C_2O	H_3^+		C_8H	
HCCN	C_5N	H_2COH^+		H_2C_6	
CH_3	SH	HC_3NH^+		SiC_3	
SiCN		CH_2D^+			

ing to conditions ripe for many high-temperature chemical reactions. Like grain surface chemistry, reactions within the shock chemistry environment are difficult to simulate, but are progressing toward a physical framework which can be compared to observations. While OH and H_2O are prominent products of ion-molecule chemistry as well as shock chemistry, SiO, and SiS are predominently produced in shocks.

In non-quiescent regions, the chemistry is generally time-dependent. This means that the chemical abundances of many molecules are a function of time and evolutionary state of the parent molecular cloud. With a more thorough understanding of the chemical processes at work in the interstellar medium, studies of the abundances of interstellar molecules will in future be coupled to the physical evolution of the interstellar medium to allow a better determination of the ages of various types of processes which occur in the interstellar medium.

A fundamental role played by molecules in the interstellar medium is as one of the cooling catalysts for the star formation process. Molecular clouds which exceed the maximum stable mass for a cloud with only thermal support, known as the Jeans mass (see §3.1), are predicted to gravitationally collapse. In order for this collapse to proceed, molecules and dust are required to radiate away energy released by the gravitational collapse. Many of the stars formed will eventually produce novae and supernovae, which further enrich the interstellar medium with molecules which can be used as catalysts to future star formation events.

9 Solar System

9.1 The Sun

Studies of the millimeter emission from the Sun have concentrated on the identification and characterization of the non-thermal millimeter emission produced by solar flares. Only the most energetic electrons (energies > 1 MeV) accelerated in solar flares produce millimeter emission. Millimeter interferometric observations made in recent years have shown that the electron population which produces the millimeter emission is different than the electron population which produces the keV-energy bremsstrahlung at x-ray frequencies. These observations suggest that two distinct electron acceleration mechanisms may be at work in solar flares.

9.2 Comets

Molecular spectral line and millimeter continuum measurements of comets are used to study the physical conditions within the comae and nuclei of these objects using the same basic techniques that are applied to these kinds of measurements made toward molecular clouds. In general, millimeter observations of comets are much more difficult to make given the rather small apparent angular size (generally less than $10''$) of most comets. In any event, inspired by the recent visitation by comet Hale-Bopp, which was the most massive comet ever observed, quite a few millimeter continuum and spectral line observations of comets have been made in the past decade.

For example, millimeter continuum observations of comets P/Halley and Hale-Bopp have been used to measure the dust particle properties of cometary nuclear matter. These measurements have shown that the dust particle sizes in these comets are greater than 1 mm and that the mass of dust contained in the radiating grains is $10^{10} - 10^{12}$ kg. Molecular spectral line observations of approximately 28 molecular species have been made toward a number of comets, with the recent visitation by the extremely large comet Hale-Bopp accounting for over half of these. Many of the molecules observed in comets are thought to be "parent" species, or species which were deposited onto icy grain mantles in the core during the formation of the comet. These species are released into the coma of a comet when it receives enough heating from the Sun to sublimate them into the gas phase, thus allowing them to be observable through their rotational transitions. Thus, measurements of parent molecular species in comets are a direct measure of the chemical properties of the material from which comets were made, which is thought to be the same material from which the Solar System formed. It is theorized that parent species chemically react with other parent species and atoms in the coma gas to produce other molecules, called "daughter" species. Since the intensity and distribution of a molecular species in a comet can be used to derive the physical conditions within the cometary nucleus and coma, studies of molecules in comets are a key element to an understanding of the physical structure of comets. An example of the variety in spatial distribution found in the molecular emission from comets is shown in Figure 10

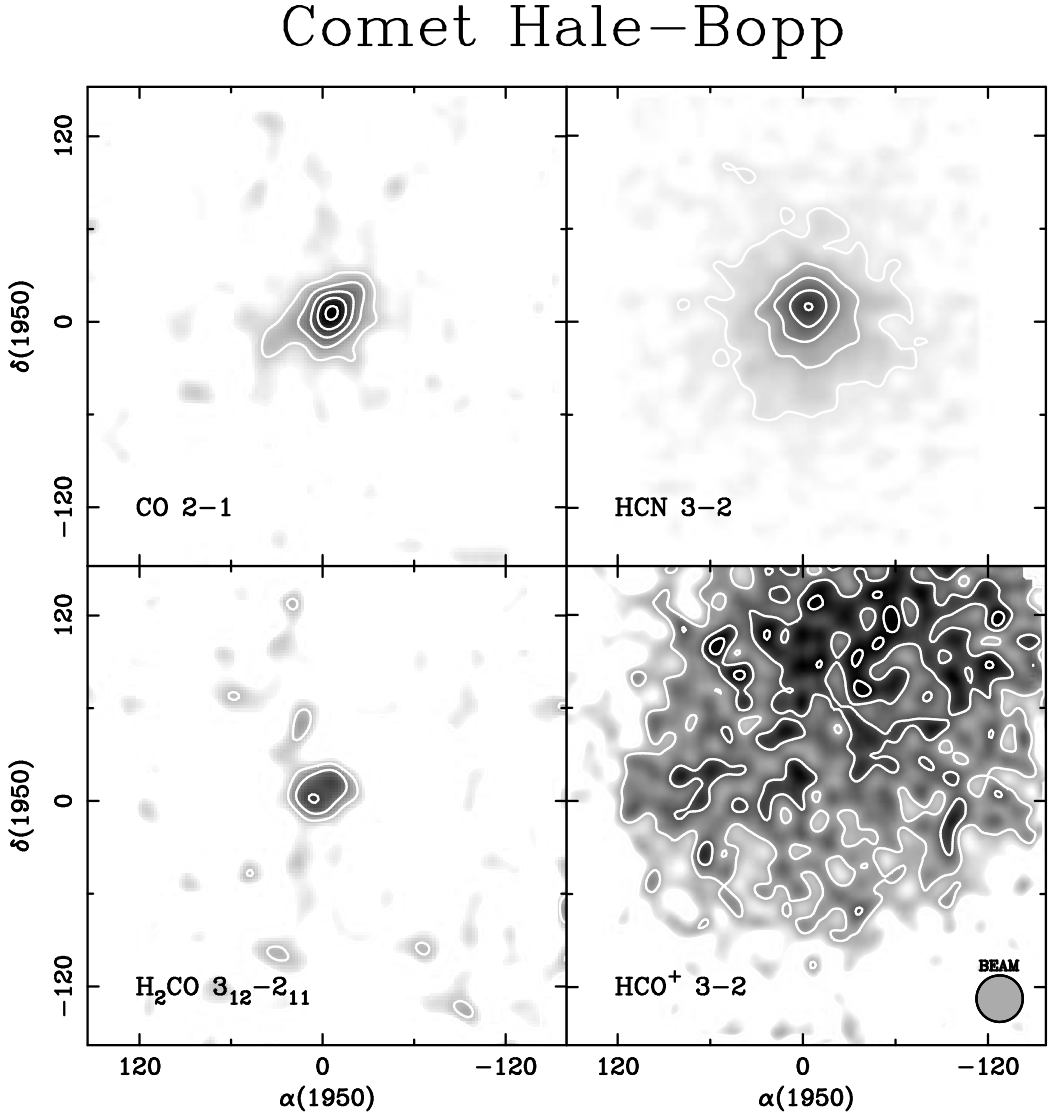

Figure 10: Spectraly integrated intensity images of the CO $2 \rightarrow 1$, HCN $3 \rightarrow 2$, H_2CO $3_{1^2} \rightarrow 2_{11}$, and HCO^+ $3 \rightarrow 2$ emission from comet Hale-Bop. Taken near perihelion in the spring of 1997, these four images reveal the chemical diversity of molecular emission from comets.

10 Planets

The millimeter wavelength emission from planets is made up of a combination of the black body continuum emission from the surface of the planet and atmospheric molecular spectral line emission. Spectral line profiles owing to millimeter wavelength molecular transitions from planetary atmospheres are used to derive its atmospheric temperature and abundance structure. Examples include measurements of CO, HDO, HCN, HC_3N, and CH_3CN from the atmospheres of Mars, Venus, Jupiter, Titan, Saturn, Uranus, and Neptune. These measurements are then used to derive the atmospheric chemistry and transport mechanisms. For example, measurements of the deuterated water (HDO) distribution in the atmosphere of Mars have been used to trace variations in the abundance of water as a function of martian latitude and season. Recent measurements point to the presence of significantly more water vapor near the north polar cap during northern summer on Mars, consistent with the sublimation of water deposits in the north polar cap. Coupled with measurements of the martian atmospheric temperature profile, the vertical atmospheric water profile has been derived. Comparison with the water vapor measurements made by the Viking lander in the 1970's indicates that the global mean water vapor content above 5 km is significantly lower today. Either the water vapor resides at very low altitudes in the martian atmosphere or the entire atmosphere is 10 times drier than it was 20 years ago.

10.1 Asteroids

Observations of asteroids at millimeter wavelengths are limited to measurements of their continuum emission. The dust emission properties from an asteroid can be used to derive the dielectric properties of its surface material, which is a direct indicator of the physical properties of the asteroid surface. This information is complementary to that which one can obtain through optical and infrared observations, but the accuracy of many of the physical measurements made using millimeter observations is often better owing to the millimeter emission process in these objects. For example, at millimeter wavelengths the absorption and emission of radiation happen in the surface layers of the asteroid at a depth of just a few wavelengths. This causes the thermal inertia to be much larger at millimeter wavelengths than it is at optical and infrared wavelengths, making the time scales for changes in the millimeter emission properties much longer (tens of hours) than the mea-

sured rotation periods of asteroids (a few hours). Another simplifying factor which makes millimeter observations more sensitive to the asteroid surface physical conditions is the fact that the emissivity at millimeter wavelengths is very close to unity. This implies that the observed brightness temperature of an asteroid is equal to its equilibrium physical temperature.

The rather simple millimeter emission properties of asteroids have made them a very attractive option for accurate flux calibration at millimeter wavelengths. Current flux calibration at millimeter wavelengths is based on models of the millimeter emission from Mars extrapolated to measurements of other planets such as Jupiter, Saturn, Uranus, and Neptune. Unfortunately, the millimeter emission from Mars is complicated by the poorly understood effects of the polar ice caps, the longitudinal dependence of the disk temperature, and the atmospheric dust storms, making the uncertainty in the Mars-based flux calibration scale 5-10%. Asteroids can provide a flux calibration standard which is accurate to better than 5%. Their small apparent angular size of less than $2''$ has limited their utility in this capacity as this angular size generally represents a small fraction of the spatial resolution of a telescope which operates at millimeter wavelengths. Advances in millimeter observing instrumentation in the next decade will overcome this limitation and further develop the use of asteroids as millimeter wavelength flux calibrators.

11 Extragalactic Astrophysics

Studies of the dust and molecular components of galaxies parallel the analyses of the physical properties in star formation regions in our own Galaxy. Most studies of the molecular and dust component of galaxies concentrate on the morphological and evolutionary impact of these components. For example, stars form within the dense molecular clouds which inhabit galactic disks, and these stars contribute significantly to the total luminosity of their parent galaxy. Measurements of the CO and dust continuum emission from a wide variety of galaxies have allowed scientists in recent years to study the global content of H_2 as a function of morphological type, luminosity, and environment in these objects. Following are some of the areas of research into extragalactic astrophysics done at millimeter wavelengths.

11.1 Mass Determination in External Galaxies

For the reasons discussed in §3.2, molecular emission is a good tracer of H_2. Since CO is the most abundant molecule after H_2, it has become the *de facto* standard for deriving the molecular mass in galaxies. The molecular mass is derived from measurements of the CO emission by first measuring the CO luminosity from a molecular cloud in a galaxy:

$$L_{CO} = D^2 \int I_{CO} d\Omega \tag{9}$$

where D is the distance to the galaxy, I_{CO} is the CO brightness temperature integrated over the line profile

$$I_{CO} = \int T_{CO} dv \tag{10}$$

and Ω is the angular size of the molecular cloud. Assuming for simplicity a spherical cloud that is in virial equilibrium, such that for a cloud of mass M_c the linewidth is given by

$$\Delta v = \sqrt{\frac{GM_c}{R}} \tag{11}$$

the cloud mass M_c is derived from the CO luminosity with the following

$$M_c = \frac{L_{CO}}{T_{CO}} \sqrt{\frac{4\rho}{3\pi G}} \tag{12}$$

where ρ is the mass density of the gas. One obtains the total CO luminosity, and therefore the total molecular mass, for a galaxy by integrating over all of the individual molecular clouds in the galaxy. A key assumption used when relating the total CO luminosity to the molecular mass is the constancy from galaxy to galaxy of the ratio $\sqrt{\rho}/T_{CO}$. Studies of this ratio in molecular clouds in our own Galaxy, in addition to studies of the CO emission from external galaxies, indicate that this factor varies by at least a factor of 2, indicating a reasonable accuracy to the proportionality between CO luminosity and molecular mass.

11.2 Morphological Studies

The spatial distribution of molecular gas in a variety of galaxies has been used to address a variety of morphological issues. Studies of spiral structure

have considered the relationships between the HI, H_2, and HII gas in spiral arms, the nature of spiral arm streaming motions, and the possible existence of higher order resonance patterns within spiral structure. One result from these studies is that in spiral galaxies the radial distributions of CO emission generally peak in the center and decrease monotonically with radius, while the atomic distributions (as traced by HI emission) in these objects show a central depression followed by a relatively constant distribution with increasing radius. An excellent example of the information available through millimeter spectral line studies of spiral arm structure in external galaxies is the image of CO $1 \rightarrow 0$ in M51 shown in Figure 11. This image shows a clear definition of the molecular gas associated with the major spiral arms in M51. A comparison with an optical image obtained with the Hubble Space Telescope shows the positional coincidence between the molecular gas and the visible dust lanes in this galaxy. The CO $1 \rightarrow 0$ imaging of M51 has revealed spiral arm molecular cloud associations with masses of $10^7 - 10^8\ M_\odot$, spatial extents of approximately 150 pc, and streaming motions in the range 20–50 km s^{-1}. Imaging studies of the millimeter dust continuum emission from M51 show a good correlation with the distribution of CO emission in this galaxy.

Barred spiral galaxies have been found to have an enhancement of CO emission along the optical bar. Additionally, many galaxies which do not show barred morphology in the optical have been found to exhibit bar-like structures in their central regions. For example, the nearby spiral galaxy IC342 contains a molecular bar, but no apparent optical bar (see Figure 12). Spiral arms which trace the locations of young stars are also apparent in high resolution imaging studies of the CO emission in these objects.

During the past 5 years morphological studies of spiral galaxies have been significantly advanced through two major millimeter interferometric surveys of the CO $1 \rightarrow 0$ emission in nearby galaxies. Using the OVRO and BIMA millimeter arrays, complete images of the CO emission from samples of 20 and 44 galaxies, respectively, were made at resolutions of 2–4″ (OVRO) and $\sim 7''$ (BIMA). Both of these surveys incorporated single antenna measurements (NRO 45m measurements for OVRO, NRAO 12 Meter Telescope measurements for BIMA) into their interferometer data to provide a complete sample of the CO emission in each galaxy. These surveys have made it possible to compare the detailed morphologies within each sample and derive physical models which describe the evolution of these morphologies. For example, the OVRO/NRO survey has found that barred spirals exhibit a higher degree of

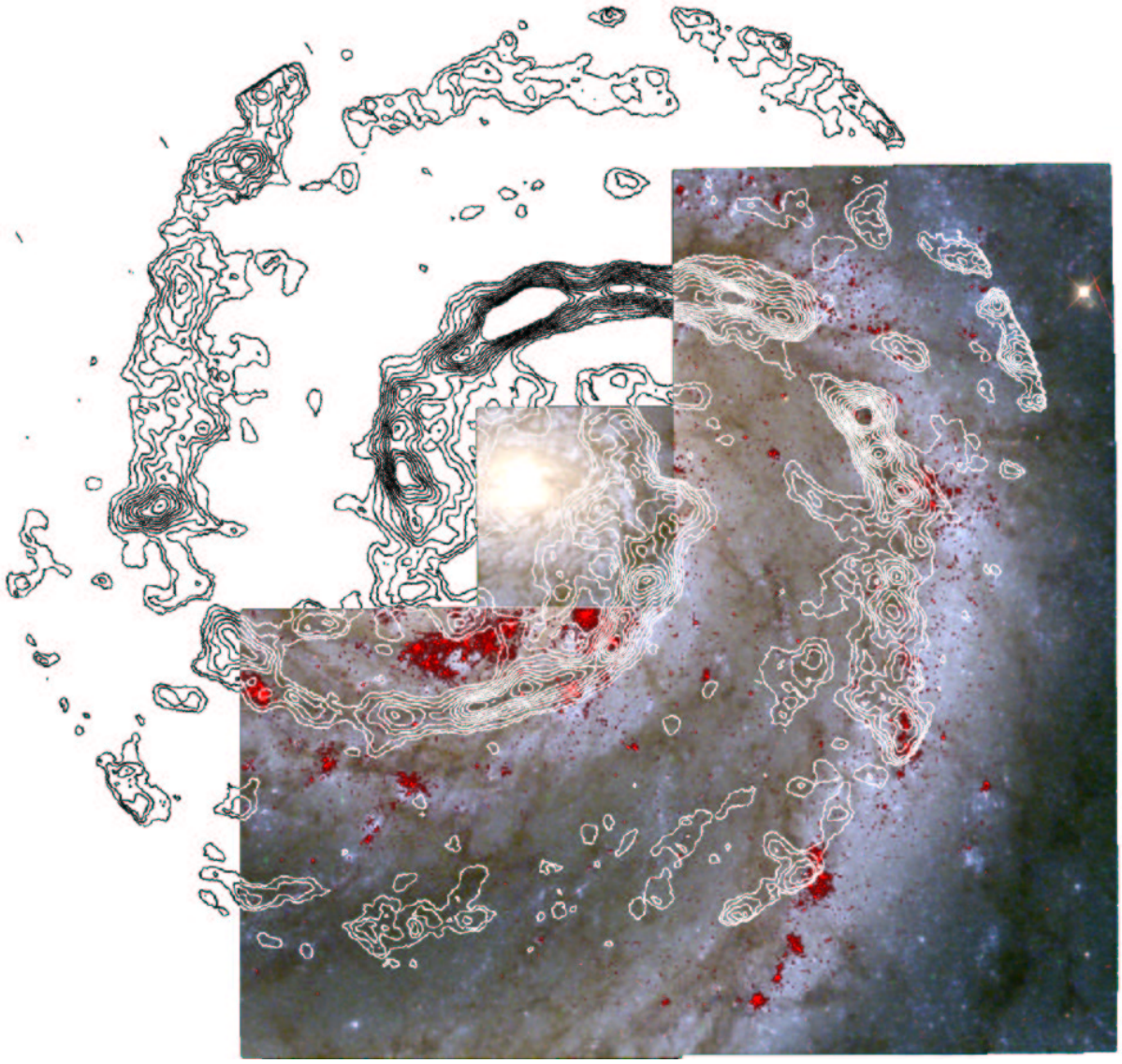

Figure 11: CO emission contours shown superimposed on a Hubble Space Telescope image of M51. The CO image, which was constructed by combining 19 individual pointings of the Owens Valley Radio Observatory millimeter array, has a resolution of 2.″3. From Aalto *et al*. 1999, ApJ, 522, 165.

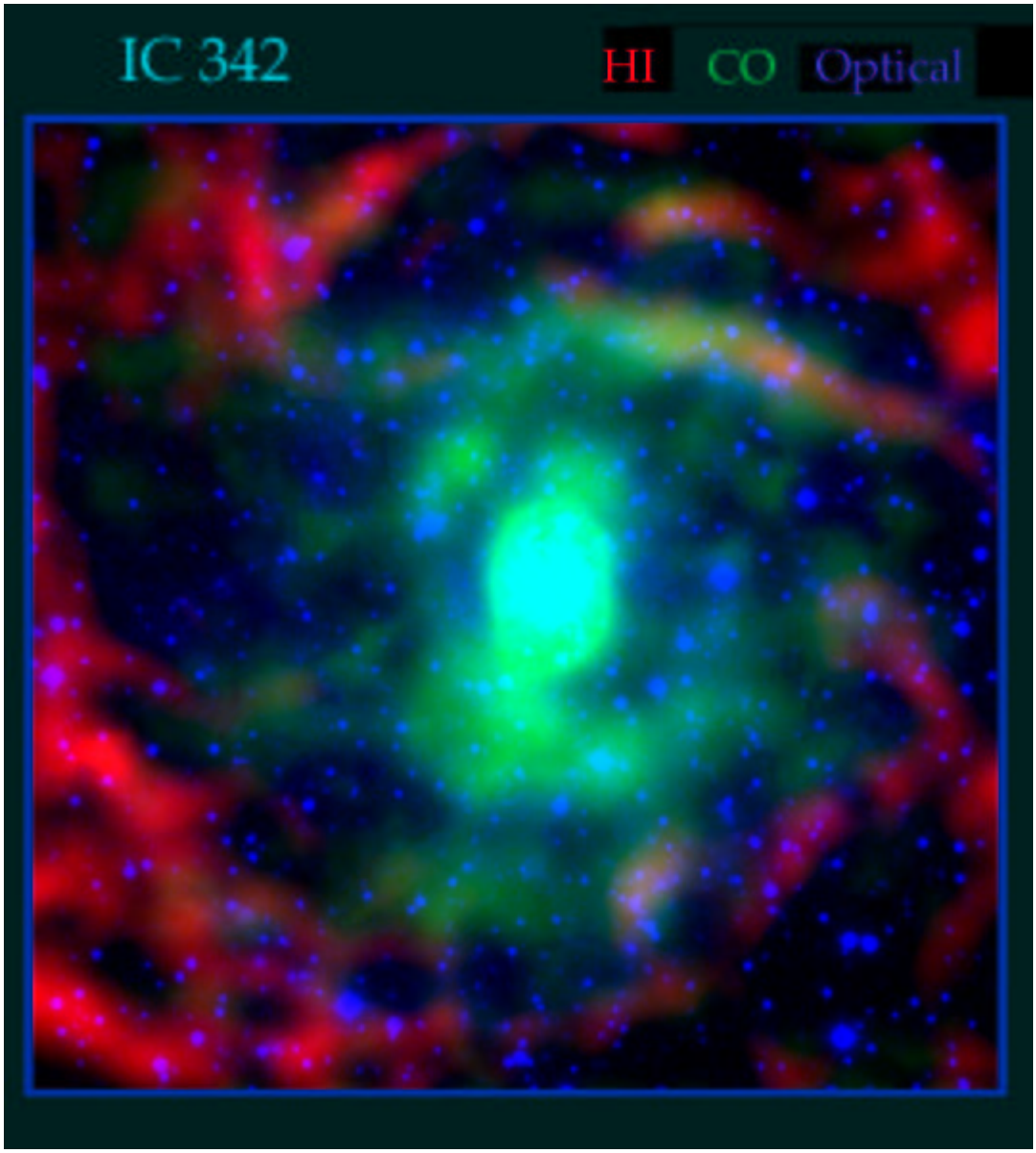

Figure 12: Overlay of the CO $1 \rightarrow 0$ (green) integrated intensity obtained using the NRAO 12 Meter Telescope, a Very Large Array HI (red) emission image, and the Palomar Observatory Sky Survey red optical image (blue) from the nearby Scd galaxy IC342. Note that the CO and optical emission coexist in the central part of the galaxy, where the HI emission is very weak. Note also that a number of spiral arms apparent in the HI emission from the outer parts of the galaxy can be traced smoothly into spiral arms apparent in the CO emission in the central parts of the galaxy. Photo courtesy of Jean Turner.

central gas concentration, but a lower overall molecular gas surface density than normal spirals. This property of barred spiral galaxies confirms theoretical predictions of rapid radial transport of gas toward the center of this type of spiral galaxy. The lower overall molecular surface density in barred spiral galaxies is thought to be caused by a more rapid expenditure of the material which feeds star formation in these galaxies.

11.3 Galactic Evolution

Studies of galactic evolution have focused on the comparison between the atomic (HI) and molecular (H_2) gas properties and star formation rates as a function of environment, luminosity, and galaxy type. The general conclusions from these studies are as follows:

1. The sum of the galactic atomic and molecular masses range from 10^6 to 5×10^{10} $M_\odot$.

2. The ratio of molecular to atomic gas mass, M_{H_2}/M_{HI}, decreases as a function of morphological type for spiral galaxy types Sa through Sd.

3. The ratio of total neutral gas mass to dynamical mass, $M_{gas}/M_{dynamic}$, increases from 4% for early type (Sa) spiral galaxies to 25% for late type (Sd) galaxies.

4. The global star formation rates and efficiencies for spiral galaxies do not show a strong dependence on morphology.

Of special consideration are galaxies which are interacting with other galaxies. Active galactic nuclei (AGN) and ultraluminous infrared galaxies (ULIRGs) represent two categories of galactic systems whose evolution has been modified by an interaction event. Galaxy-galaxy interactions are known to disrupt the stellar component of galactic disks and enhance the star formation rate. The molecular component of these systems appears also to be disrupted, leading in many cases to an order-of-magnitude increase in the star formation efficiency, with a more efficient production of massive stars.

11.4 Galactic Nuclei

The most dominant molecular component in galaxies is their nuclei. In recent years the level of sensitivity available for studies of galactic nuclei has allowed

for not only the detection of CO in these nuclei, but also studies of the spatial distribution of CO and other molecules. Studies utilizing measurements of the spatial distribution of HCN and CS from a number of nearby active galactic nuclei and starburst galaxies have resulted in a better understanding of the physical properties, kinematics, and mass distribution of the dense gas in these regions. The information gathered from these studies has also been used to investigate the relationships among various types of "active" galaxies, such as active galactic nuclei (AGN), ultraluminous infrared galaxies (ULIRGs), and starburst galaxies.

Studies of nearby galaxies have provided information on the physical properties of the dense gas in galactic nuclei which in turn have provided a useful comparison to studies of the dense gas properties in our own Galaxy. For example, the nearby starburst galaxy NGC 253 has been studied with high spatial resolution multitransition measurements of CO and HCN. The spatial distribution of the molecular clouds imaged in NGC 253 is similar to that found in the central regions of our own Galaxy, but the kinetic temperature and volume density is 100 K and $10^4 - 10^5$ cm^{-3}, warmer and denser than average Galactic molecular clouds. Similar studies of the dense gas distribution and properties in other nearby galaxies such as M82, NGC 1068, and M51 have yielded comparative information useful in defining the detailed physical characteristics of these galaxies.

11.5 High Redshift Galaxies

Important constraints on the evolution of galaxies have been provided by the search for and characterization of distant galaxies. These searches, conducted using CO as a tracer of molecular gas, have pointed to the existence of massive quantities of dust and molecular gas out to redshifts as high as 4.69. This high redshift corresponds to ages within a few billion years of the Big Bang, thus indicating enrichment of molecular gas through chemical processing at a very early epoch. Currently 12 galaxies have been measured with redshifts greater than 2. Imaging studies of these objects have provided information on their gas and dynamical mass, information which cannot be gleaned from observations at other wavelengths. The gas mass fraction in these systems is used as a measure of their evolutionary state, providing a constraint on the epoch of initial star and galaxy formation. A characterization of the physical properties of high redshift systems is also being used to establish whether galaxies formed hierarchically or as systems which were given their present

day masses during formation.

11.6 Cosmology

In addition to the cosmological implications of studies of the millimeter emission properties of galaxies, the structure of the cosmic microwave background radiation (CMBR) and direct measurements of the Hubble constant H_0 have been made using millimeter astronomical techniques. The recent measurements of the Sunyaev Zel'dovich effect (SZE) toward a sample of 27 clusters using 26-36 GHz receivers on the BIMA and OVRO millimeter arrays have provided some of the most direct measurements of several cosmological parameters. The SZE is the spectral distortion of the CMBR owing to inverse Compton scattering of photons by electrons in hot gas confined to the deep gravitational potential produced by galaxy clusters. A fundamental property of SZE emission is that the observed brightness is a function of the cluster properties and is independent of its distance. Therefore, SZE measurements can yield a very accurate measure of the Hubble constant H_0 and the matter density of the universe Ω_M. Current results from these SZE measurements indicate that $H_0 = 67$ km s^{-1} Mpc^{-1} and $\Omega_M h_{100} \sim 0.25 \pm 0.06$ (h_{100} is the Hubble constant normalized to a value of 100 km s^{-1} Mpc^{-1}). Note that the distance-independent nature of these SZE measurements makes them the most accurate way in which to measure H_0 and Ω_M astronomically.

Bibliography

André, P., Ward-Thompson, D., and Barsony, M. (2000). *From Pre-Stellar Cores to Protostars: The Initial Conditions of Star Formation.* In Protostars and Planets IV (V. Mannings, A. P. Boss, and S. S. Russell, eds.), in press. University of Arizona Press, Tucson, AZ.

Bachiller, R. (1996). *Bipolar Molecular Outflows from Young Stars and Protostars.* Annual Reviews of Astronomy and Astrophysics 34, 111–154.

Butler, B. J. and Gurwell, M. A. (2000). *Solar System Science with ALMA.* In Science with the Atacama Large Millimeter Array (A. Wootten, ed.), in press. Astronomical Society of the Pacific, San Francisco, CA.

de Pater, I. (1990). *Radio Images of the Planets.* Annual Reviews of Astronomy and Astrophysics 28, 347 399.

Evans, N. J., II (1999). *Physical Conditions in Regions of Star Formation.* Annual Reviews of Astronomy and Astrophysics 37, 311 362.

Neininger, N. (1999). *Interferometric Observations of Nearby Galaxies.* In The Physics and Chemistry of the Interstellar Medium (V. Ossenkopf, J. Stützki, and G. Winnewisser, eds.) GCA Verlag, Herdecke, Germany.

Sargent, A. I. and Welch, W. J. (1993). *Millimeter and Submillimeter Interferometry of Astronomical Sources.* Annual Reviews of Astronomy and Astrophysics 31, 297 343.

Scoville, N. Z. and Sargent, A. I. (2000). *Imaging Spectroscopy at mm-Wavelengths.* In Imaging the Universe in Three Dimensions: Astrophysics with Advanced Multi-Wavelength Imaging Devices (W. van Breugel and J. Bland-Hawthorn, eds.). ASP Conference Series volume 195, pp. 236 247.

Turner, B. E. 1992. *Interstellar Medium, Molecules.* In The Astronomy and Astrophysics Encyclopedia (S. Maran and C. Sagan, eds.). The Astronomy and Astrophysics Encyclopedia. van Nostrand, p. 378.

van Dishoeck, E. F. and Blake, G. A. (1998). *Chemical Evolution of Star-Forming Regions.* Annual Reviews of Astronomy and Astrophysics 36, 317 368.